Urban Ecosystems (2023) 26:525–546
https://doi.org/10.1007/s11252-022-01321-9

Space–time analysis of the earth's surface temperature, surface urban heat island and urban hotspot: relationships with variation of the thermal field in Andalusia (Spain)

David Hidalgo García[1] · **Julián Arco Díaz**[1]

Accepted: 16 December 2022 / Published online: 20 January 2023

Abstract
Understanding just how the increase in the Earth's Surface Temperature (LST) is related to alterations of the urban climate —Surface Urban Heat Island (SUHI) or Urban Hotspots (UHS)— and with the deterioration of cities´ environmental quality has become a great challenge. Societies worldwide seek actions that might break these trends and improve the quality of life of local inhabitants in the face of climate change. In this research, and with the help of Sentinel 3 satellite images (day and night), the space–time variability of the LST and the SUHI over the metropolitan areas of the capitals of Andalusia (Spain) during the year 2021 was studied to evaluate how these variables, together with the Land Use/Land Cover (LULC), may have influenced the variability of the UHS and the level of thermal comfort according to the Thermal Field Variance Index (UTFVI). As results, an important spatial variability of the LST, SUHI, UHS, and the different classes of UTFVI is reported. The diurnal UHS are found mainly in rural areas without vegetation, whereas the night UHS are distributed in urban areas with impervious surfaces.

Keywords Land surface temperature (LST) · Surface urban heat island (SUHI) · Landsat · Urban hotspots (UHS) · Urban thermal field variance index (UTFVI) · Land use indices

Introduction

In recent years, extreme weather events tied to climate change have been acknowledged as a most urgent challenge facing society (Kovats et al. 2005; Song et al. 2020).

Highlights
- Spatio-temporal variability (day and night) of the LST, SUHI, UHS and UTFVI variables is reported.
- The highest daytime LST values are seen for rural areas as opposed to urban ones, where the highest nighttime LST values are reported.
- Daytime UHSs are concentrated in rural areas; nighttime UHSs are concentrated in cities.
- In daytime readings, classes 2 and 3 of the UTFVI predominate, whereas classes 3 and 4 predominate in night readings.
- There is evidence of a correlation between the LST, SUHI and UHS variables in both day and night readings.

✉ David Hidalgo García
dhidalgo@ugr.es

Julián Arco Díaz
juliannn@ugr.es

[1] Technical Superior School of Building Engineering, Fuentenueva Campus, University of Granada, Granada 18071, Spain

Land modification through the expansion of urbanized areas due to population growth is one of the processes that most contributes to climate change (Li et al. 2011). Currently, according to a report by the United Nations, 50% of the world´s population is urban; and it is expected to increase to 70% by 2050 (UNO 2018). Thus, in the next 30 years, an increase of 2,500 million inhabitants (Mukherjee and Singh 2020) will mean an increase in impervious surfaces toward a coverage of more than 1,500,000 km^2 (Schneider et al. 2010).

It is known that urban development is the main driver of economic and urban growth, implying an expansion of industry and transport, but it alters the urban microclimate through an increase in the Land Surface Temperature (LST) (Scolozzi and Geneletti 2012; Song et al. 2020). Recent studies have reported a positive correlation between urban areas and LST and a negative correlation between it and green areas: rural areas have lower temperatures than urban ones, but urban green areas have somewhat lower temperatures than urban ones (Hua et al. 2020; Karakuş 2019; Tsou et al. 2017; Yang et al. 2020a). The greatest increases in temperature are mainly due to the phenomenon called Urban Heat Island (UHI), which produces a modification

whose intensity is heightened by society (Santamouris 2020). Other studies have confirmed that the UHI generates a series of climatic and economic problems in society, bearing an impact on the quality of life of people living in cities (Dwivedi and Mohan 2018; Macintyre et al. 2018; Rozos et al. 2013).

To determine such phenomena, remote sensing stands out among the different methodologies available. It allows for large-scale urban studies of LST, UHI, UTFVI and different Land Uses/Land Covers, or LULCs (Song et al. 2018) by means of satellite images with infrared sensors (TIRS). To understand the effects that variations in the coverage of urban areas can have on the LST and the SUHI, it is essential to analyze land use and cover (Tepanosyan et al. 2021).

In short, changes in urban land cover cause changes in the microclimate, which in turn affect the physical and mental well-being of the inhabitants of urban areas (Das and Das 2020). Spain is one of the European countries showing the greatest development of artificial coverage or built-up area. It is therefore necessary to ascertain the consequences of high temperatures for the everyday life for Spanish citizens, and report results that may be extrapolated to other geographic realms.

The Urban Thermal Field Variance Index (UTFVI) is commonly used by the scientific community to assess the thermal quality of urban areas. It can identify high temperature spaces called Urban Hot Spots (UHS) (Amindin et al. 2021; Das and Das 2020; Sharma et al. 2021) and determine their association with LULC. Recent research has concluded that UHS are found within urban areas having higher UHI intensities and which correspond to areas of higher LST. These studies warn of significant increases in the LST of urban areas during the past decade, directly linked to an increase in UHS (Amindin et al. 2021; Luo and Wu 2021; Sharma et al. 2021). A study on the industrial development authority of New Okhla (India) between the years 2011 and 2019 reports respective LST and UHS increases of 6.4 K and 33.56% (Sharma et al. 2021); a study on the city of Ahvaz (Iran) between 1995 and 2018 likewise reported increases in LST and UHS of 3 K and 4%, respectively (Amindin et al. 2021); a study involving five districts of the Suez Governorate area (Egypt) between 1988 and 2014 reported increases of 4.5 K in the LST and 16% in the areas classified as UHS (Ahmed 2018).

Most of the studies to date refer to the LST obtained through one or several satellite images selected with the sole criterion of having low cloud cover. The UHS and UTFVI index of the investigated area are derived from the values of that or those days. Hence the results of these studies correspond to the chosen day or days and to the time of passage of the satellite, which are extrapolated to longer periods with the aim of proposing global mitigation and resilience measures. This is an erroneous premise, as some studies underline the high variability of the LST and UHI both throughout the day and over time (Anjos et al. 2020; Emmanuel and Krüger 2012; Hidalgo and Arco 2021). Establishing effective climate change mitigation and resilience measures in urban areas therefore calls for knowing the space–time variability of the UHS and the UTFVI index. For this reason, it is vitally important to work with images that orbit a point on the earth's surface several times a day (Sentinel 3 or Modis).

The objective of this research is to study the space–time evolution experienced by the UHS and the UTFVI index and look into their relationships with the LULC over the metropolitan areas of eight cities in the region of Andalusia (southern Spain) during the year 2021. To this end, and using Sentinel 3 images (day and night), LULC maps were generated, the LST was recovered, the SUHI was obtained, the evolution of the UHS was explored, and the UTFVI of the areas evaluated was investigated. Finally, statistical analysis served to determine correlations between the data obtained and the variables of study, using the Data Panel technique. The research questions that we intend to answer are the following: 1. Do the UHS and the UTFVI index of the areas under study present any time–space variability throughout the day? 2. Is there any relationship between the LULCs and the areas identified as UHS? 3. Could the results obtained in this research improve the measures and guidelines for the future urban planning of the cities of Andalusia?

Materials and methods

Study area

The area under study pertains to the eight development plans of the subregional territory of the capitals of Andalusia, specifically the cities: Huelva, Cadiz, Sevilla, Malaga, Cordoba, Jaen, Granada and Almeria (Fig. 1). Andalusia has a population of 8,427,325 and an area of 1,213,742 Ha, being the second largest region in Spain and the most populated one. The region features somewhat diverse background climates. According to the Koppen-Geiger climate classification, Malaga, Sevilla, Jaen and Cordoba feature a Mediterranean climate (Csa), the cities of Huelva and Cadiz share a Mediterranean Oceanic climate (Csb), and Almeria and Granada have a cold semi-arid climate (Bsk).

Overall, Andalusia has hot, dry summers and mild, humid winters (de Castro et al. 2007). The region borders on the Mediterranean Sea to the south and mountains to the north. They act as a shield from the sea breezes. The average altitude is 503 m above sea level. The number of hours

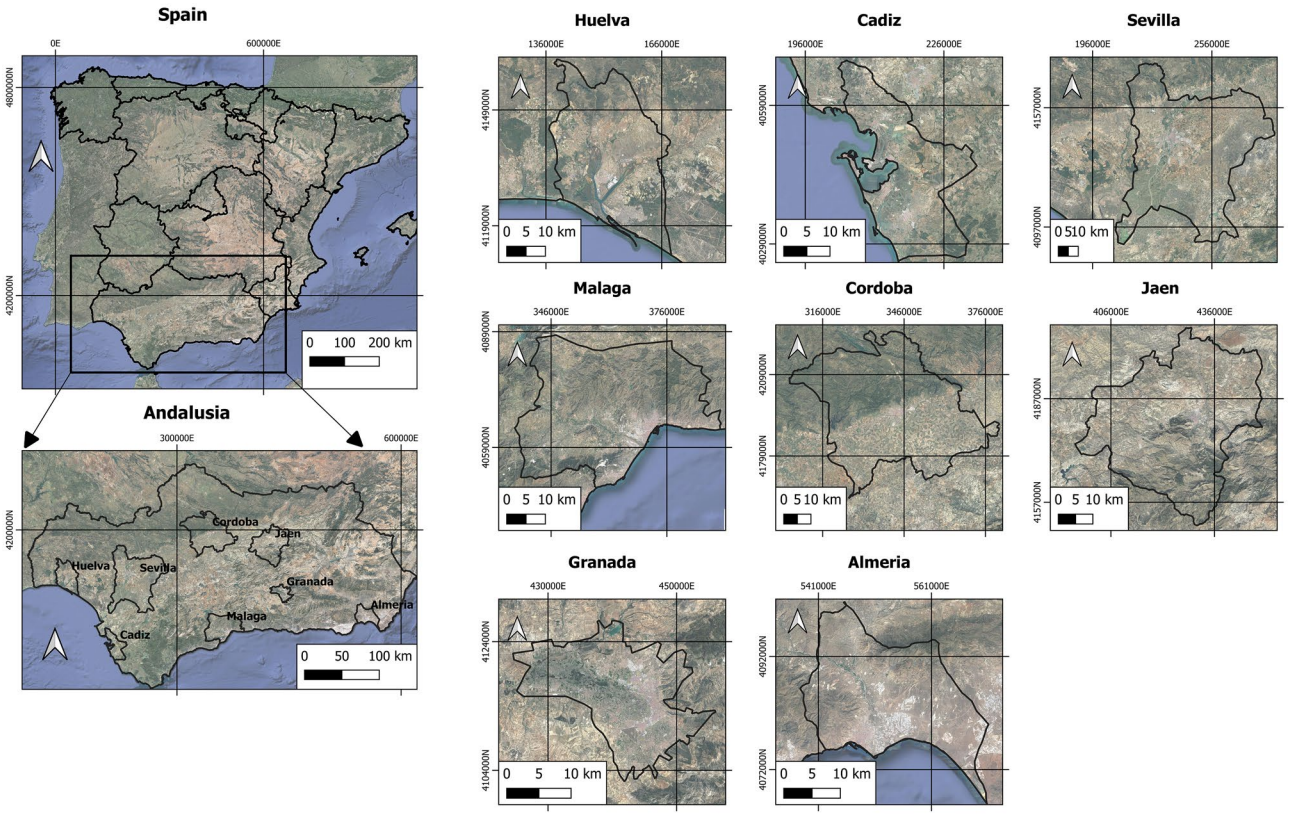

Fig. 1 Study area: Andalusia, Spain

of sunshine per year ranges between 2,900 and 3,100, giving an average of 7 to 8 h of sunshine per day. The average annual temperature fluctuates between 300 K in July and 284 K in January, with a maximum in summer of 317 K and a winter minimum of 270 K. Table 1 displays the regional characteristics.

Methodology

The methodology carried out for the development of this research work is described in Fig. 2.

Through Sentinel 3A and 3B images, the day and night LST for the year 2021 was determined. This information was transferred to the open-source software QGIS, version 3.16.16. The LST and LULC images were acquired through ESA's Copernicus Open Access Hub for level 2. The determination of land cover relied on a precision matrix to ensure accuracy; the area to be assessed underwent cross-tabulation between the reference category and the classified one (Campbell 1996). Its use in studies that require the classification of the land surface is well documented (Xu et al. 2009; Yoo et al. 2019). Next, the SUHI was determined, and the diurnal and nocturnal UHS and UTFVI of the area under study were identified with the Raster calculator tool of the indicated software. Specialized software for data science, STATA version 16, was used for statistical analysis.

Sentinel 3 images

The Sentinel 3 s features a high-resolution scanning instrument, the Land Surface Temperature Radiometer. Sentinel 3 Tier 2 products allow for direct and automatic download of Land Surface Temperature (LST) along with associated parameters such as Normalized Vegetation Index (NDVI), Land user/Land cover (LULC), Proportion vegetation (PV), and the normalized difference index (NDBI). In Sentinel LSTR level 2 processing, a LULC map is stored as an auxiliary data file containing a high spatial resolution of the vegetation and cover type.

The images used were acquired through ESA's Copernicus Open Access Hub for level 2 and with a cloudiness level of less than 15% to ensure accuracy of the pixel values of the LST and the subsequent calculation of SUHI. The selected images correspond to twenty-four days in the year 2021. They were distributed equally between the months of January and December. The general schedule for the satellites to pass over Andalusia is between 10:00 and 11:00 a.m. and 21:00 and 22:00. In this way, 48 images have been used, 24 pertaining to the morning and 24 to the evening.

Table 1 Characteristics of the cities of Andalusia

Geographic information	Sevilla	Cordoba	Jaen	Granada	Huelva	Cadiz	Malaga	Almeria
Downtown location UTM	37.375 N, -6.025 W	37.891 N, -4.819 W	37.780 N, -3.831 W	37.111 N, -3.362 W	37.270 N, -6.974 W	36.516 N, -6.317 W	36.765 N, -4.564 W	36.841 N, -2.492 W
Climate Zone	Csa	Csa	Csa	Bsk	Csb	Csb	Csa	Bsk
Mean annual T. (K)	291.7	290.9	290.5	288.6	291	291	291.6	291
Average annual rainfall (mm)	576	612	552	450	467	597	520	228
Total area (Ha)	397,042	266,028	168,370	35,806	96,885	60,553	133,015	56,043
Total urban area (Ha)	6869	3135	943	2178	1487	734	5860	1495
Population in 2021 (hab)	1,548,741	1,528,000	222,844	541,465	235,003	639,098	1,007,331	270,415
Urban mean elevation (masl)	11	106	570	680	24	13	8	16

The first stages of processing entailed reclassification at a resolution of 100 m, atmospheric correction using the Sentinel 3 Application Platform (SNAP) Toolbox, and georeferencing using the ETRS89/UTM Zone 30 N projection system. Sharpening, allowing the resolution to be changed from 1000 to 100 m, was performed with the TsHARP algorithm, which relies on a linear regression model. Both highly precise and simple to apply, it is commonly used by the scientific community for this type of study (Agam et al. 2007a, b; Huryna et al. 2019).

Land surface temperature estimation (LST)

The Sentinel algorithms that allow for obtaining the LST are based on the concept of absorption difference (McMillin 1975), according to which it is possible to correct the atmospheric effects by means of the difference between the two wavelengths of the TIRS band. Previous studies establish the precision and validation of these algorithms in Sentinel-3 images (Ruescas et al. 2016). The algorithm of the product SLSTR Sentinel internally includes the emissivity of the land according to the following equation (Pérez et al. 2021; Remedios and Emsley 2012):

$$LST = a_{f,i,pw} + b_{f,i}(T_{11} - T_{12})^{\frac{1}{\cos\left(\frac{\theta}{m}\right)}} + \left(b_{f,i} + c_{f,i}\right)T_{12} \quad (1)$$

where LST is the temperature of the Earth's surface in degrees K; a, b and c are the ground cover coefficients; and T_{11} and T_{12} are the brightness temperatures in the upper part of the atmosphere on bands 8 and 9, respectively. Subscript f corresponds to the vegetation fraction; i denotes vegetation type; and pw is the atmospheric column´s water vapor content. In turn, θ is the zenith angle of view of the satellite located in the metadata file, while m is a dependent variable of θ (Remedios and Emsley 2012; Yang et al. 2020b).

Sentinel 3 products with processing level 2 allow for direct determination of the LST, as the application of the algorithm (1) is performed internally by the open-source Sentinel Application Platform (SNAP) software. After determining the LST of the investigated cities, data were exported in raster images using QGIS software.

Surface urban heat island estimation

According to the literature, the SUHI is derived from the temperature difference between measurements made simultaneously in the urban area and the rural area (Oke 1987). Therefore, the SUHI can be determined according to Eq. 2:

$$SUHI = LST_{urban} - LST_{rural} \quad (2)$$

The urban LST values correspond to the average values of the pixels located within the urban area. The rural areas chosen to derive the SUHI correspond to places where the Spanish State Meteorological Agency (AEMET) has a rural weather station, generally 15–16 km outside the cities, and having no paved areas within a radius of 1000 m. Using the raster

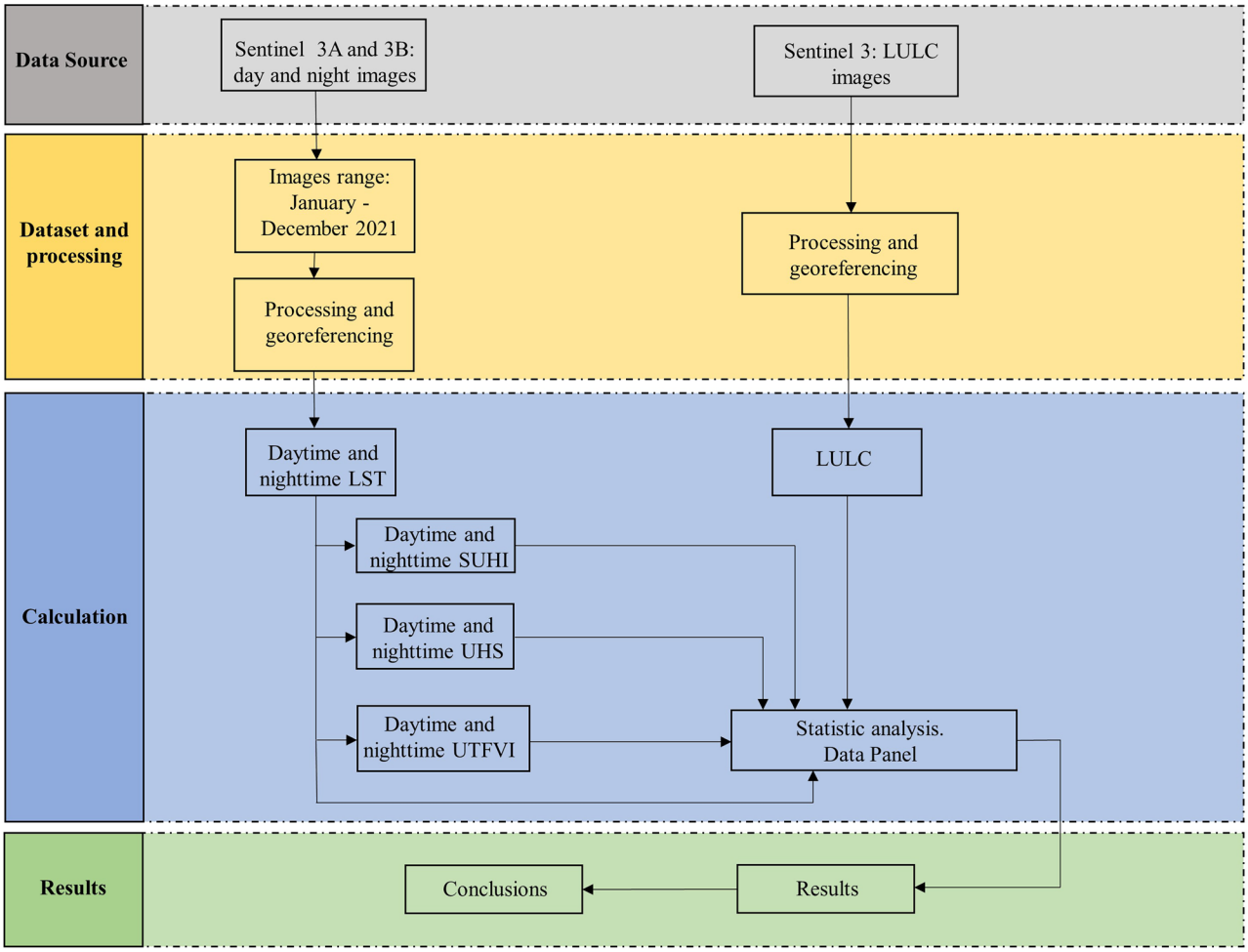

Fig. 2 Methodology

calculator command of the QGIS software and the exported Landsat images, the SUHI of Granada was determined by Eq. 2.

Urban hotspots (UHS)

Hot spots are identified based on the LST within the study area. They are zones of variable size found within places giving the highest temperatures, and they are usually considered as uncomfortable for human activity. These spaces are determined using the following formula (Guha 2017; Sharma et al. 2021):

$$LST > \mu + 2 * \sigma \tag{3}$$

where μ and σ are respectively the mean value and the standard deviation of the LST of the zone in ºC. Using this equation, the areas that present urban zones with LST values above the mean and with a confidence interval greater than 95% can be determined.

Urban thermal field variance index (UTFVI)

This index allows the value of each pixel of the urban area to be appraised in relation to the entire area, so as to obtain a classification of environmental quality (Sobrino and Irakulis 2020). The UTFVI values fall into six typologies, in turn presenting six classes of ecological evaluation (Tables 9 and 10). Each is related to the degree of presence of the SUHI phenomenon and its impact on the environmental quality of the population (Liu and Zhang 2011). The UTFVI classes, based on the strength of the SUHI, range from 1 (excellent) to class 6 (worst), determined using the following equation (Guha et al. 2018):

$$UTFVI = \frac{LST - T_{mean}}{T_{mean}} \tag{4}$$

where LST is the temperature of each pixel (K) and T_{mean} is the average LST of the entire area (K). UTFVI values below zero indicate a complete absence of the UHI phenomenon,

signalling maximum thermal comfort, hence an area classified as affording excellent environmental quality. As UTFVI values increase, SUHI intensity also increases, so that thermal comfort deteriorates (Sharma et al. 2021).

Strategy of analysis

Panel data refers to statistical analysis that combines a temporal dimension (time) with a cross-sectional dimension (data or values). This method is often cited in the literature and involves the use of multiple regression models (Alcock et al. 2015; Chen et al. 2011; Fang and Tian 2020), which allows for a larger amount of data to be included than under traditional methods. There are three calculation options: ordinary squares method (OSM), generalized least squares (GLS), and intragroup estimation method (IEM) (Labra 2014). To ascertain which of these three should be applied, the following steps must be carried out (Chen et al. 2011). 1) Using the Hausman test, determine if the effects of the analysis are fixed or random; this allows the method to determine different hypotheses about the behaviour of the residuals of statistical analysis. 2) Evaluation of the model using the Wooldridge and Wald tests. These stages will indicate the most appropriate method to be used (Seto and Kaufmann 2003). Our statistical analysis was performed with STATA software, version 16. After carrying out the indicated tests, the GLS method with random effects was used according to Eq. 5.

$$Y_{it} = \beta X_{it} + \alpha_i + \mu_{it} \quad (5)$$

where μ_{it} is the error of the model, α_i represents the individual effects, X_{it} are explanatory variables, β is an independent variable, t = time and i = individual.

Results

LULC analysis

Analysis of the coverage of the studied areas is represented in Fig. 3 and Table 2.

In general, the coverage with the largest area is called sparse vegetation, with an average value of 33.3%; mosaic cropland occupies an average value of 18.6%, and shrubland an average value of 13.5%. In contrast, the coverages having the smallest areas would be flooded vegetation with an average value of 0.4%, grassland with an average value of 0.5% and closed broad-leaved deciduous forest and mosaic grassland, each with an average coverage of 0.7%.

These values reflect the vegetation and crops typical of regions by the Mediterranean Sea basin, and fit the climate types of the Köppen-Geiger classification. Seen in Table 3 are the results of the precision matrix carried out to verify the LULC maps obtained. The precision was 80%, with a 95% confidence interval that varies between 0.77 and 0.89 points. The Tau value is 0.783; the Kappa coefficient obtained is 0.815. After determination of the matrix, however, manual correction was applied to the points that did not coincide with the LULC maps obtained using Sentinel 2 satellite images.

Spatio-temporal evaluation of LST

Figures 4 and 5 show the space–time analysis of the day and night LST of the areas studied.

Table 4 presents the measures of central tendency and dispersion of both variables. The mean maximum daytime values range between 304.2 K for the city of Cordoba and 308.3 K in the city of Almería. The average diurnal minimum values range between 291.4 K in Jaen and 298.1 K in Huelva. The average daytime values vary between 299.6 K in the cities of Jaen and 302.9 K in the city of Almeria. Daytime LSTs are higher in coastal cities (301.8 K) than for inland cities (300.6 K). The highest LST values are reported in rural areas, whereas the lowest values of LST occur in urban areas.

The mean maximum night values range between 293.2 K for the city of Sevilla to 291.2 K for Huelva. The mean night minimum values range between 284.2 K in the city of Malaga and 287.6 K in Sevilla. The average night values vary between 286.8 K in Huelva and 285.9 K in Sevilla. Nocturnal LSTs are observed to be higher in inland cities (288.1 K) as opposed to coastal cities (287.9 K). Overall, the highest LST values are reported in urban areas, the lowest values corresponding to rural areas.

Spatio-temporal evaluation of SUHI

Figures 6 and 7 show the space–time analysis of the day and night SUHI of the areas under study.

Table 5 presents the measures of central tendency and dispersion of the SUHI. The mean maximum daytime SUHI values range between 6.4 K in Cadiz and 1.8 K in the city of Granada. The average diurnal minimum values range between -7.7 K in the city of Jaen and -1.9 K for Huelva. In turn, the average daytime values range from 2.5 K for Huelva to 0.1 K for Sevilla. Daytime SUHI values are found to be higher in coastal areas (1.4 K) than inland areas (0.8 K). As with the LST, the highest SUHI values are seen for rural areas, and the lowest in urban areas.

The mean maximum night values of SUHI range between 4.0 K in the city of Cadiz and 1.7 K in Granada. The mean minimum night values range from -3.8 K for Malaga to -0.7 K for Huelva. The average night values are between 0.3 K in the city of Malaga and 1.7 K in Jaen. Nocturnal

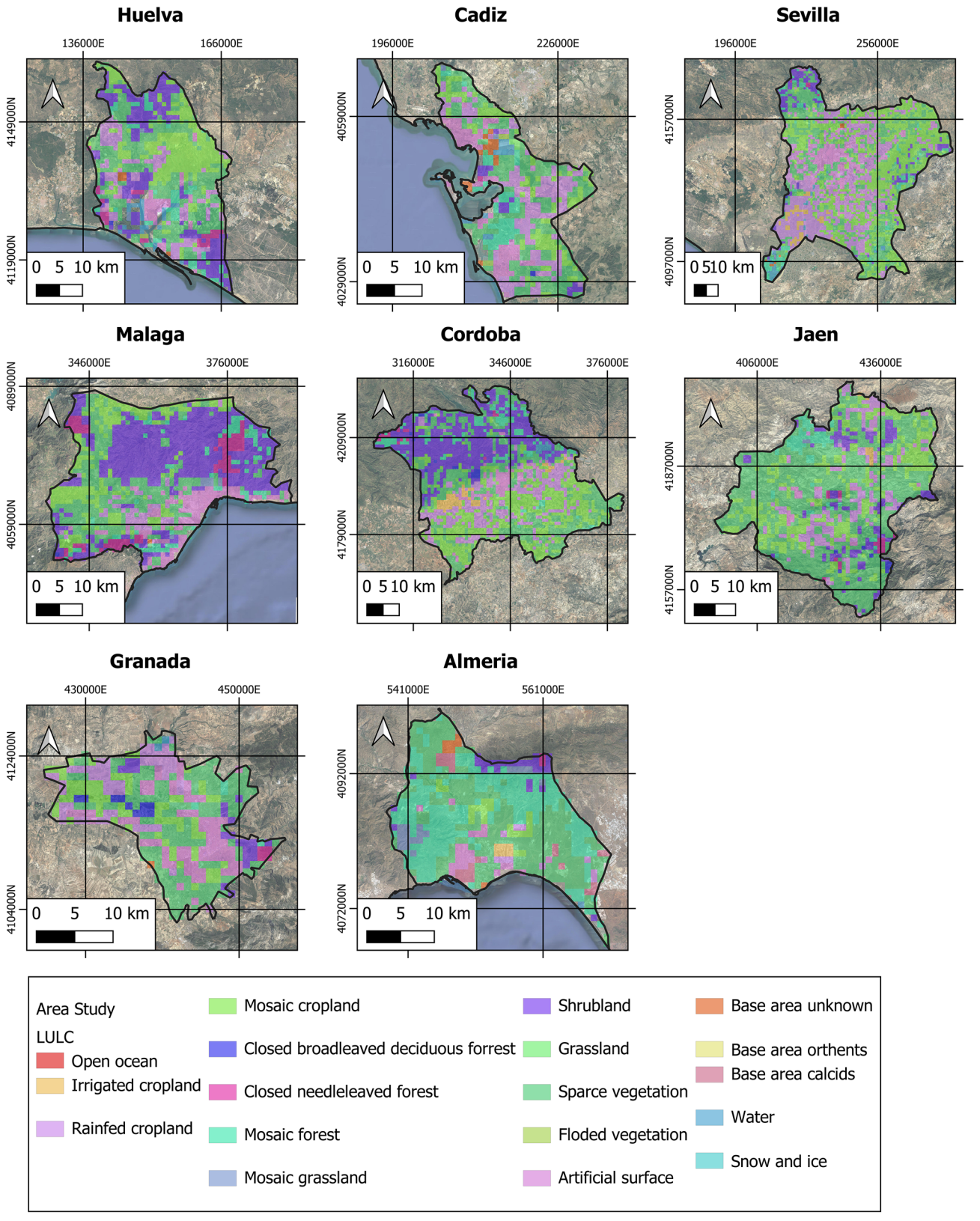

Fig. 3 LULC coverage of the areas under study

Table 2 Land cover of the areas under study

LULC (%)	Granada	Cordoba	Jaen	Sevilla	Huelva	Cadiz	Malaga	Almeria
Water	0.5	0.7		1.3	2.3	2.4		0.2
Closed needle-leaved forest	1.0	0.7	0.9	0.1	2.6	0.2	6.0	0.3
Irrigated cropland		2.2	0.5	1.7				1.0
Base area unknown	0.3			0.2	0.5	2.4	0.1	1.2
Rainfed cropland	14.3	13.7	10.8	27.8	11.4	22.9	3.6	1.7
Mosaic grassland		0.0	0.2	0.1	0.3	0.3	0.6	3.1
Base area calcites								3.8
Mosaic cropland	17.9	23.5	19.8	32.9	21.5	15.5	14.1	3.8
Artificial surface	19.1	4.3	4.7	3.3	4.4	11.2	8.5	4.0
Shrubland	5.6	24.1	6.9	5.1	20.6	2.5	39.1	4.3
Mosaic forest		5.5	3.5	3.3	5.7	7.6	5.7	36.5
Sparse vegetation	38.8	24.4	52.2	24.1	30.5	33.8	22.3	40.3
Closed broad-leaved deciduous forest	2.6	0.9	0.5		0.1	0.2	0.1	
Grassland						0.5		
Flooded vegetation					0.2	0.6		

SUHI are higher in inland areas (1.0 K) as opposed to coastal areas (0.7 K). As occurs with the nocturnal LST, the highest SUHI values are reported in urban areas, whereas the lowest SUHI values occur in rural areas.

Spatio-temporal evaluation of UHS

Figures 8 and 9 offer space–time analysis of the day and night UHS of the areas under study.

Table 6 presents the measures of central tendency and dispersion. In general terms, the area occupied by daytime UHS zones is seen to oscillate between 8.1% in the city of Cordoba (21614 ha) and 32.9% in the city of Huelva (31906). The average value of extension of the diurnal UHS zones in the studied areas is 21.2%. However, extension of UHS zones is greater in coastal cities (25.1%) than in inland cities (17.3%). The UHS, like the high LST, pertains to rural areas as opposed to urban areas, where UHS areas are barely identified.

Deserving mention with regard to nocturnal UHS is the wide range: between 3.1% for the city of Seville (12500 ha) to 26.1% for Jaen (43978 ha). The average value of the extension of the nocturnal UHS zones in the studied areas is 14.4%. Yet again, the extension of the UHS zones is greater for coastal cities (15%) than inland ones (13.7%). The UHS also tend to be located in urban areas rather than rural areas.

Next, the day and night zones identified as UHS were extracted and related to the LULC coverage plan. This was done to determine if certain coverage types are more closely linked to high temperatures and located within the areas catalogued as UHS. The results, given in Tables 7 and 8, indicate that during the morning UHS zones are concentrated in areas having coverage without vegetation, in crop areas, scrubland, and rainfed areas. In contrast, surfaces identified as forest or man-made surface are not within UHS zones. Table 8 shows how, at night, the areas identified as UHS correspond to artificial surface coverage, zones without vegetation, and scrub. Areas identified as forest, grassland, or cropland are not within UHS zones.

Evaluation using UTFVI

Figures 10 and 11 offer the space–time analysis of the day and night UTFVI evaluation of the study areas.

Tables 9 and 10 show the variability of each of the UTFVI zones. In general terms, the areas under study present two major UTFVI surfaces. During the morning, areas 2 (23.5%) and 3 (35.9%) predominate. The areas with the best ratings (1: excellent, 2: good, and 3: normal) are located in urban areas; the areas with the worst ratings (4: bad, 5: worse, and 6: worst) are located in rural areas. Contrariwise, according to night readings, areas 3 (49.0%) and 4 (25.5%) predominate. The areas with the best ratings are rural, and those with the worst ratings are urban. The variability of the zones between the day and night measurements is as follows: 1 (-17.3%), 2 (-4.5%), 3 (13.1%), 4 (9.4%), and 5 (-0.7%).

Statistical analysis

Relationship between LULC and LST

The statistical analysis carried out was of great importance to arrive at correlations between the day and night LST and the LULC land cover in the areas under study. First, the Pearson

Table 3 Precision matrix

	1	2	3	4	5	6	7	8	9	10	11	12	13	14	15	UA (%)
1	20	0	0	0	0	0	0	0	0	0	0	0	1	1	0	90
2	0	20	0	0	0	1	0	0	1	0	0	0	0	0	0	90
3	0	0	20	0	2	0	0	0	0	0	1	1	0	0	0	80
4	0	0	5	20	0	2	0	0	0	0	0	0	2	1	0	50
5	0	0	0	2	50	0	0	2	0	1	1	1	0	0	0	86
6	0	0	0	0	0	20	0	0	0	0	0	1	1	0	0	90
7	0	0	0	0	0	0	20	0	0	0	0	0	0	0	0	100
8	1	1	1	0	0	0	0	100	2	3	2	5	1	0	0	84
9	2	2	1	0	0	0	0	1	60	0	0	3	2	1	0	80
10	0	1	0	0	0	0	0	2	3	100	2	3	1	1	1	86
11	0	0	0	0	0	0	0	1	1	1	60	2	1	1	1	87
12	0	3	0	0	1	1	0	1	1	0	0	100	3	0	0	90
13	1	2	1	0	2	2	0	0	0	0	1	1	20	0	0	50
14	2	0	1	0	3	1	0	0	0	1	1	0	0	20	0	60
15	1	0	1	0	0	0	0	0	0	0	0	0	0	0	20	90
PA (%)	65	55	50	90	84	65	100	93	90	94	87	83	40	75	90	650

1. Water, 2. Closed needle-leaved forest, 3. Irrigated cropland, 4. Base area unknown, 5. Rainfed cropland, 6. Mosaic grassland, 7. Base area calcites, 8. Mosaic cropland, 9. Artificial surface, 10. Shrubland, 11. Mosaic Forest, 12. Sparse vegetation, 13. Closed broad-leaved deciduous forest, 14. Grassland, 15. Flooded vegetation. PA (15): Producer accuracy. UA (15): User accuracy

correlation coefficient was determined, then the Data Panel was developed. For the latter, the Generalized Least Squares (GLS) method was applied through Eq. 5. Results are indicated in Tables 11 and 12.

In general, the LULC shows strong correlations with the LST. In the case of the daytime LST, the correlation is negative (-0.685) while for the nighttime LST the correlation is positive (0.710). The results of the statistical analysis using the Data Panel technique signal a statistically significant and negative relationship of 95% between the LULC variable and the diurnal LST, yet they give a statistically significant and positive relationship of 99% with the nocturnal LST variable. The values of R^2, F statistic and Prob > chi^2 obtained show good concordance between the dependent variable and the independent ones used, with an adjustment level greater than 99% significance.

Relationship between LST and SUHI

The results of the data analysis between the LST and the day and night SUHI are indicated in Tables 13, 14 and 15.

As observed, the daytime LST presents a strong positive correlation with the daytime SUHI (0.715), while the nighttime LST also presents a strong positive correlation with the nocturnal SUHI (0.642). The rest of the possible relationships show low correlation.

The results of the statistical analysis using the Data Panel technique report a statistically significant and positive relationship above 99% between the daytime LST and SUHI variables and between the nighttime LST and SUHI variables. The values of R^2, F statistic and Prob > chi^2 obtained show good agreement between the dependent variable and the independent ones used, the adjustment level being higher than 99% significance as Prob > chi^2 = 0.000.

Relationship between UHS and LST, SUHI and LULC

The results of the data analysis are indicated in Tables 16, 17 and 18.

In general, diurnal UHS values present strong positive correlations with diurnal LST (0.659) and diurnal SUHI (0.872), but a very weak relationship with LULC (-0.011). On the contrary, the nocturnal UHS present strong positive correlations with the nocturnal LST (0.703) and the nocturnal SUHI (0.823), and a weak relationship with the LULC (0.176).

According to our statistical analysis using the Data Panel, there is a statistically significant and positive relationship above 99% between the diurnal and nocturnal UHS and SUHI variables. The diurnal and nocturnal UHS and LST variables report a positive relationship of 95%. The values of R^2, F statistic and Prob > chi^2 obtained show good concordance between the dependent and independent variables used, with an adjustment level of 99% significance, since Prob > chi^2 > 0.000.

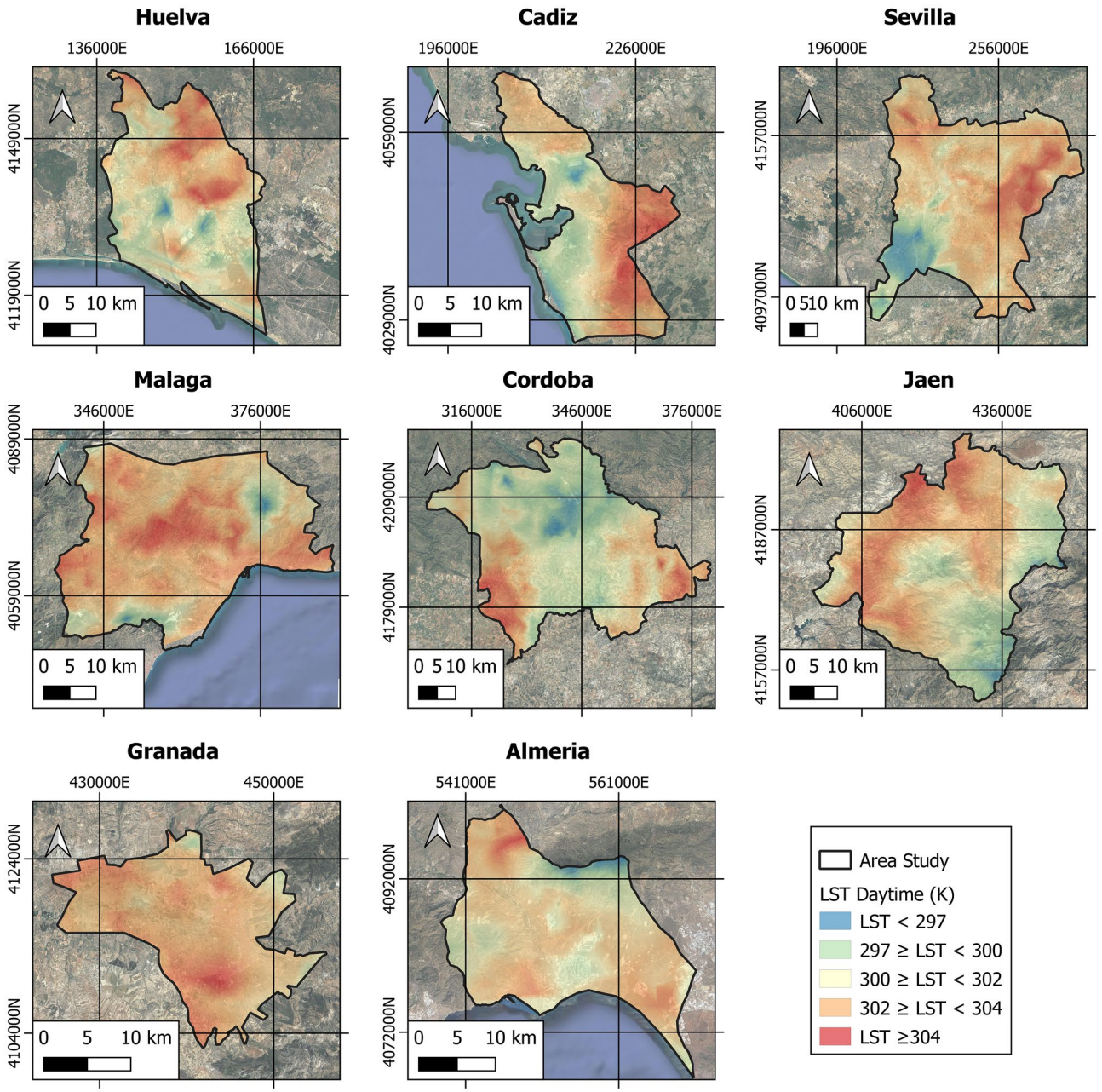

Fig. 4 Variability of the diurnal LST of the area studied

Discussion

This study focuses on the space–time variability of the LST, SUHI, UHS and UTFVI during the year 2021 in the "urban agglomeration areas" of the capitals of Andalusia, furthermore exploring the relationship between the LST and the LULC index. Our aim to determine the spatial variability of the UHS and UTFVI variables between day and night readings was intended to yield a global vision of climate change implications, perhaps pointing the way to useful mitigation measures for the future.

In the Mediterranean region studied here, the average daytime LST is clearly seen to be higher in rural than in urban areas. This circumstance is motivated by the fact that in the early hours of the morning solar radiation is lower in urban areas than in rural areas. This is

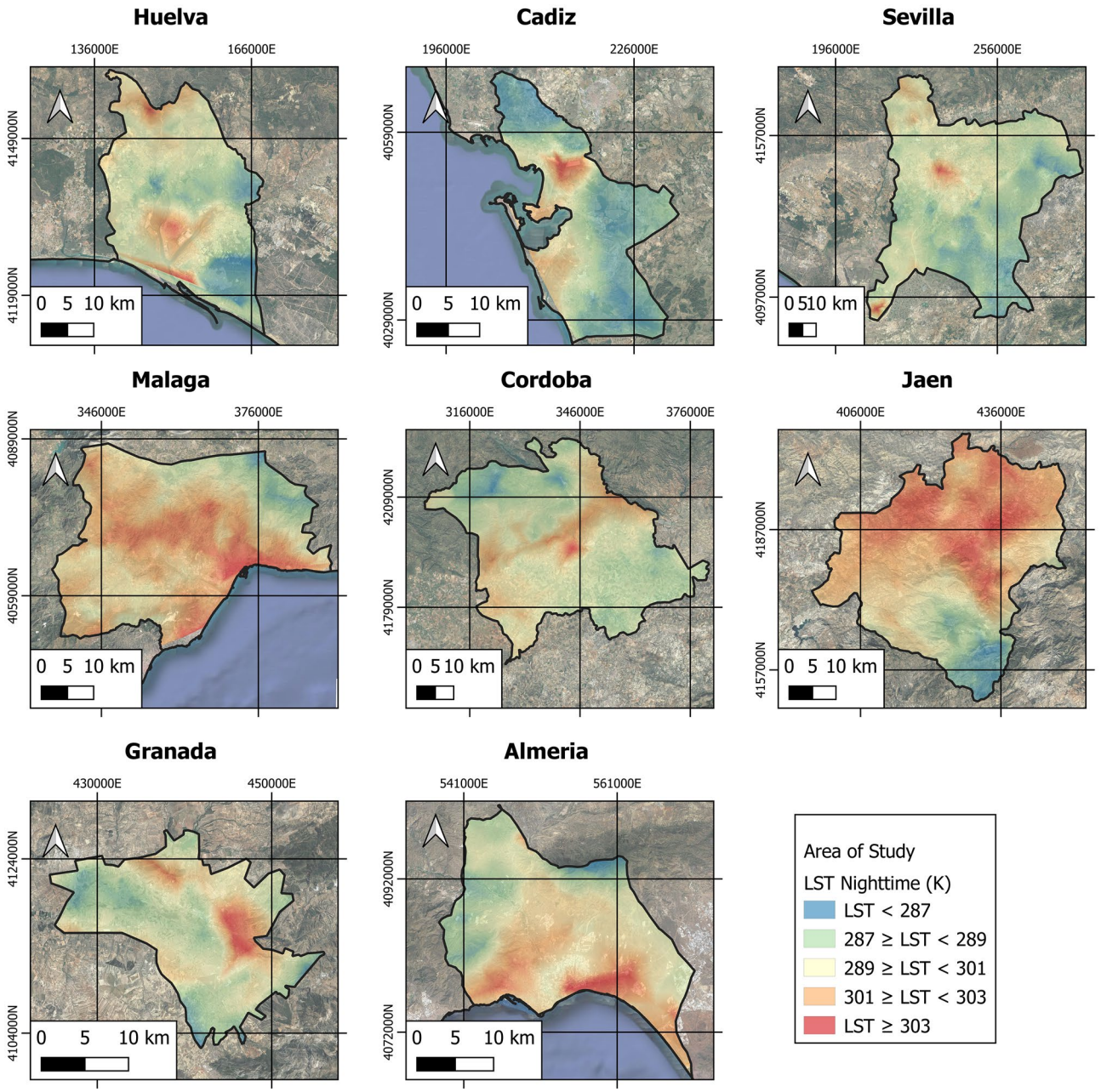

Fig. 5 Variability of the nocturnal LST of the studied area

Table 4 Dispersion measures of daytime and nighttime LST

	LST Daytime (K)				LST Nighttime (K)			
	Max	Min	Mean	SD	Max	Min	Mean	SD
Huelva	305.6	298.1	300.7	1.1	291.2	287.3	286.8	0.7
Cadiz	305.4	294.9	301.1	1.0	293.0	287.2	288.8	1.1
Sevilla	306.6	297.3	302.1	1.0	293.2	287.6	289.5	0.8
Malaga	307.4	297.9	302.6	1.2	291.5	284.2	287.5	1.3
Cordoba	304.2	294.9	298.9	2.1	292.2	286.8	288.6	0.8
Jaen	304.6	291.4	299.6	1.2	292.7	285.9	287.9	1.3
Granada	304.1	295.9	299.6	1.3	293.0	284.6	286.6	0.7
Almeria	308.3	297.6	302.9	1.1	291.6	286.3	288.5	0.8

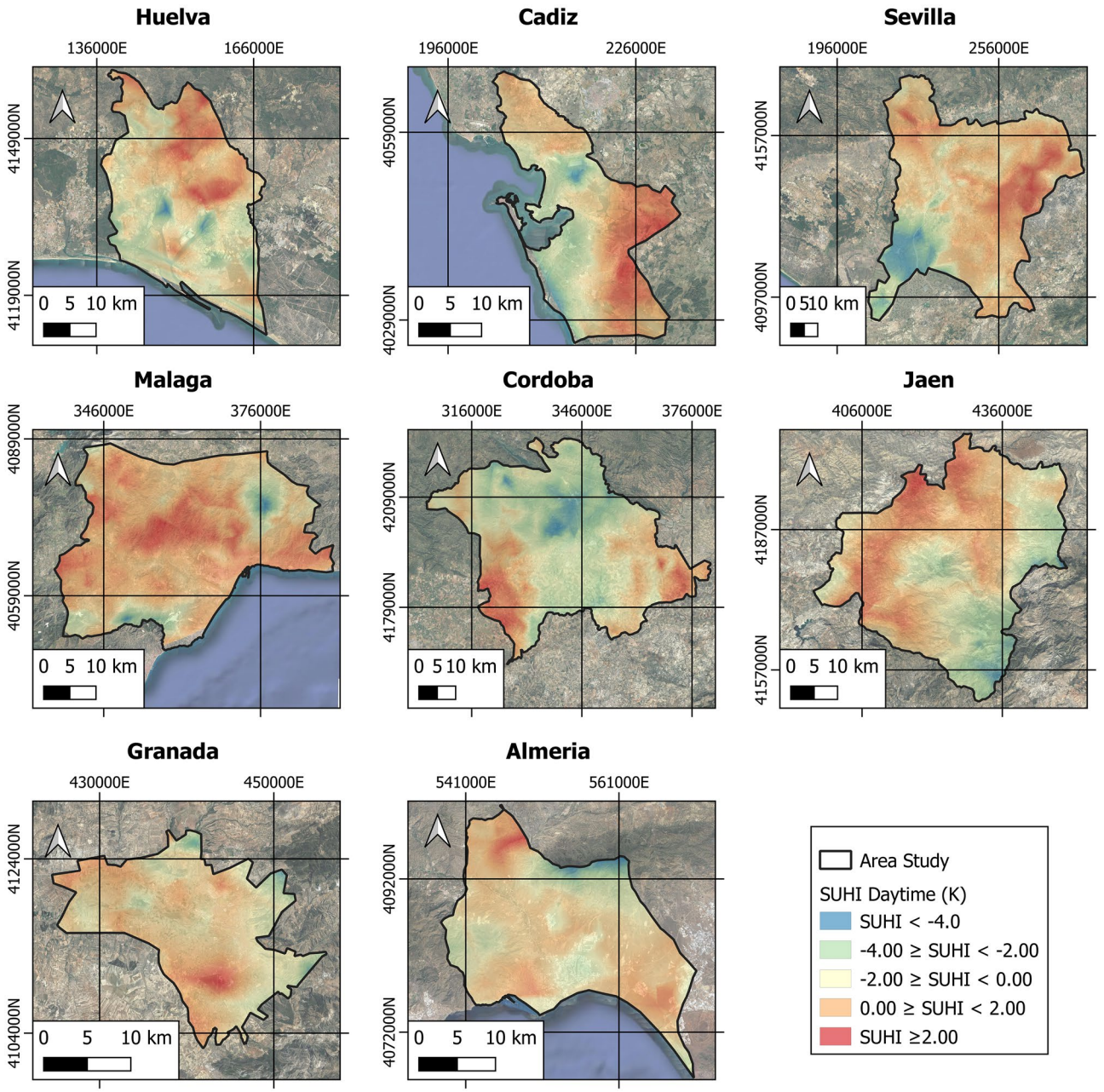

Fig. 6 Variability of the diurnal SUHI of the studied areas

due to the fact that shade is generated by buildings and trees, to the heterogeneous system of impermeable walls and great thermal absorption, and to the cooling rates undergone by areas with vegetation, as well as the heating rates of areas with scarce vegetation and bare soil. In this way, the buildings and trees in the city create shade that prevents solar radiation from heating up the impermeable walls of urban areas, and hence from later giving off high doses of heat and altering the LST of the area (Lemus et al. 2020; Li and Meng 2018; Yang et al. 2020a). In turn, numerous studies carried out with satellite images have shown that the vegetation of urban areas has a cooling effect (Du et al. 2020; Lin et al. 2015; Qiu et al. 2017), which ranges between 1 and 3 K, whereas in areas with little vegetation and/or bare soil, heating occurs. These effects occur not only due to the rates of

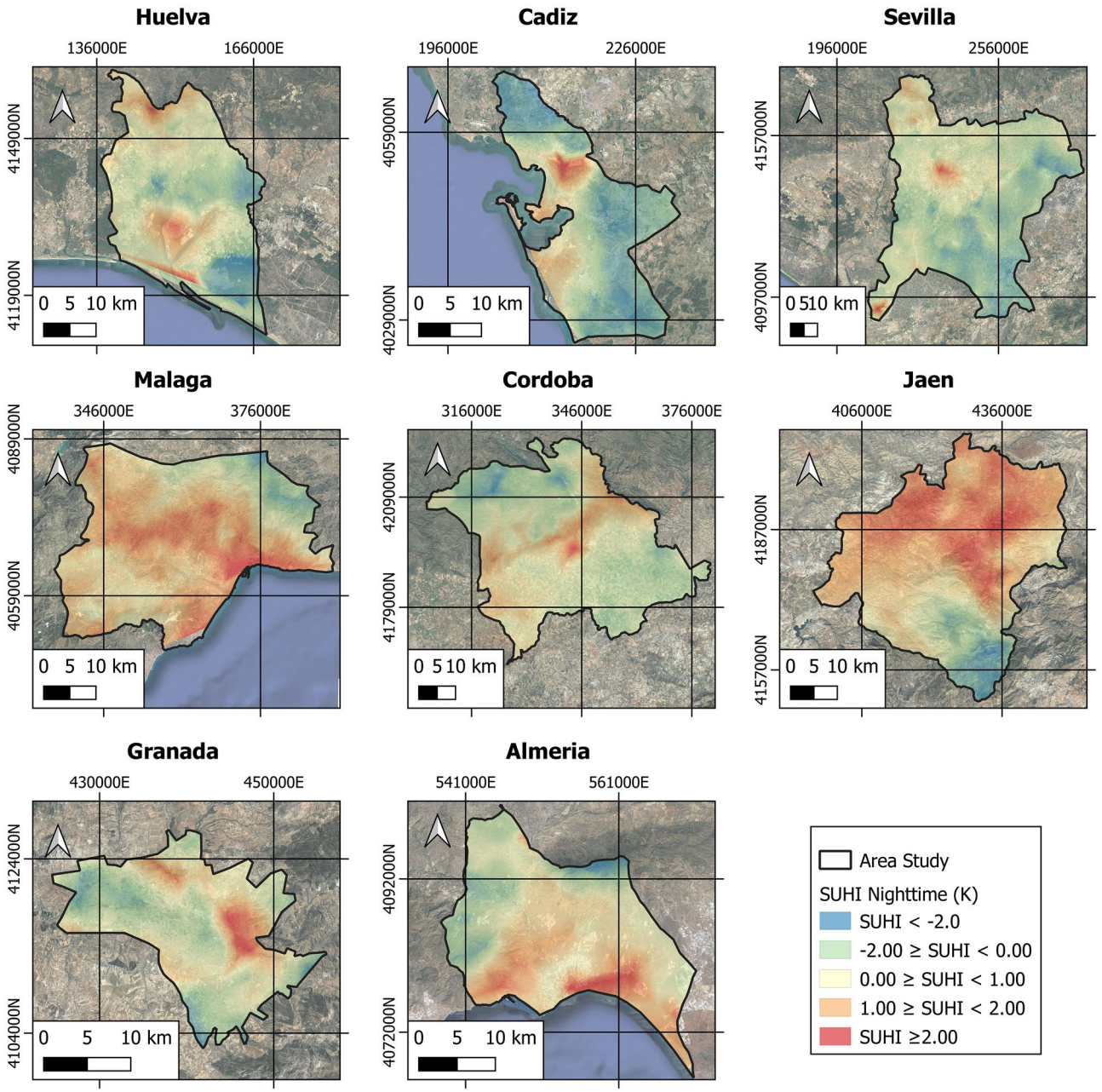

Fig. 7 Variability of the nocturnal SUHI of the studied areas

Table 5 Diurnal and nocturnal SUHI dispersion measurements

	SUHI Daytime (K)				SUHI Nighttime (K)			
	Max	Min	Mean	SD	Max	Min	Mean	SD
Huelva	5.4	-1.9	2.5	1.1	3.2	-0.7	1.0	0.7
Cadiz	6.4	-4.1	2.2	2.2	4.0	-1.8	0.4	1.2
Sevilla	3.5	-5.7	0.1	1.8	3.2	-2.4	0.5	0.8
Malaga	4.5	-8.1	0.8	1.8	2.5	-3.8	0.3	1.1
Cordoba	6.2	-4.4	0.9	2.1	3.2	-2.2	1.2	0.8
Jaen	5.6	-7.7	0.4	2.5	3.7	-2.1	1.7	1.3
Granada	1.8	-3.4	0.3	0.3	1.7	-1.7	1.2	0.6
Almeria	4.3	-6.4	0.3	1.4	3.6	-1.7	1.1	1.0

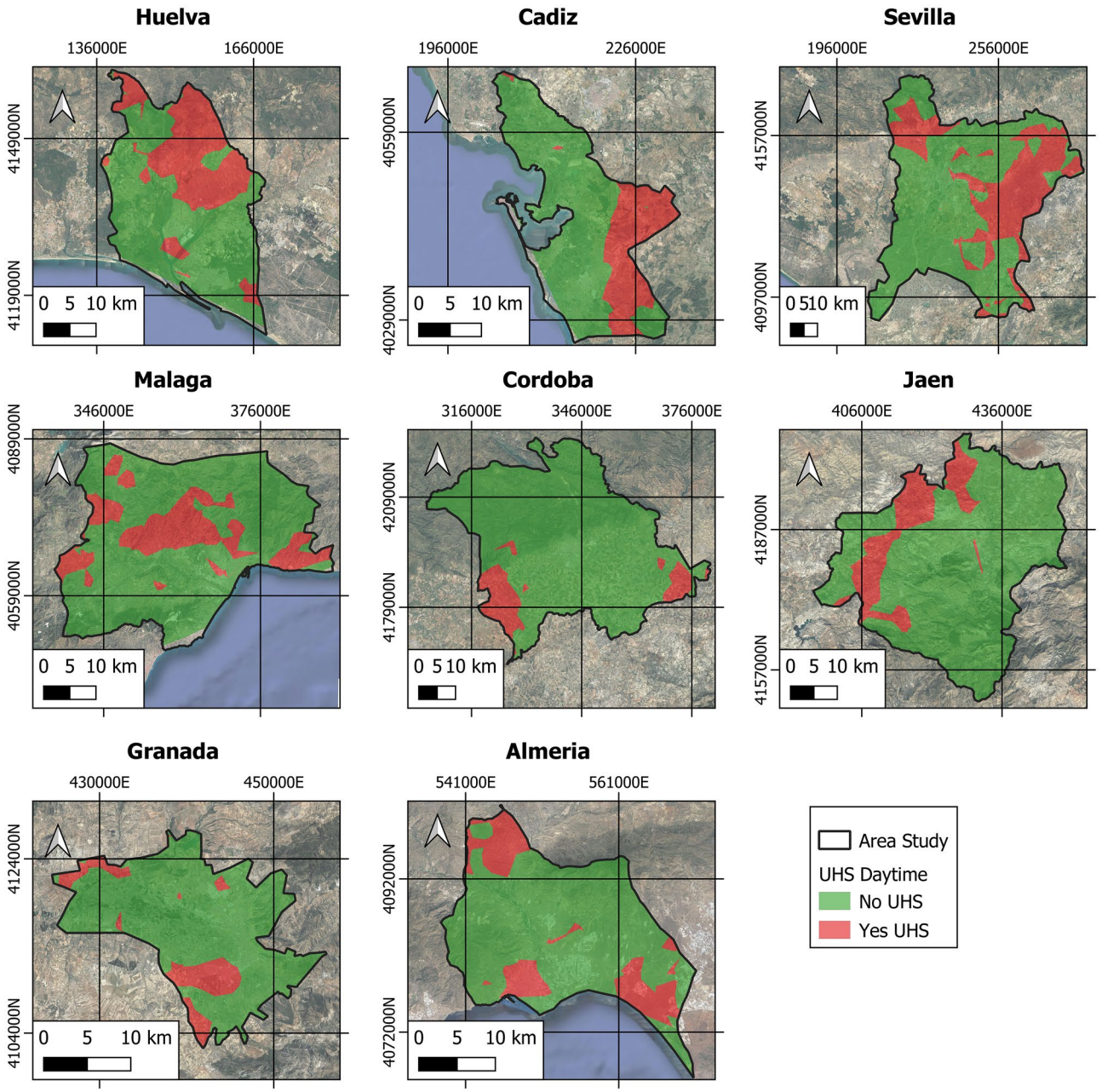

Fig. 8 Variability of the diurnal UHS of the studied areas

cooling and heating by convection and transpiration, but can also be attributed to the processes of shading and evapotranspiration that would alter the LST of the zones. Contrariwise, the reason why the average night LST is lower in rural areas than in urban areas is that once the sun goes down, the former tends to cool quickly, but the building materials of the latter retain heat. The use of waterproof materials with high thermal absorption inside cities turns them into reservoirs of heat —in the afternoons they give off the heat absorbed during the day. This situation, previously studied by other authors, is now known as an urban heat island (Saaroni et al. 2018; Wu et al. 2019; Yang et al. 2020a).

Considerable spatial variability of the areas classified as UHS is evidenced between the day and night data of the areas studied. This is clearly motivated by the spatial range in terms of LST and SUHI values already outlined, corroborated through statistical analysis. Strong positive

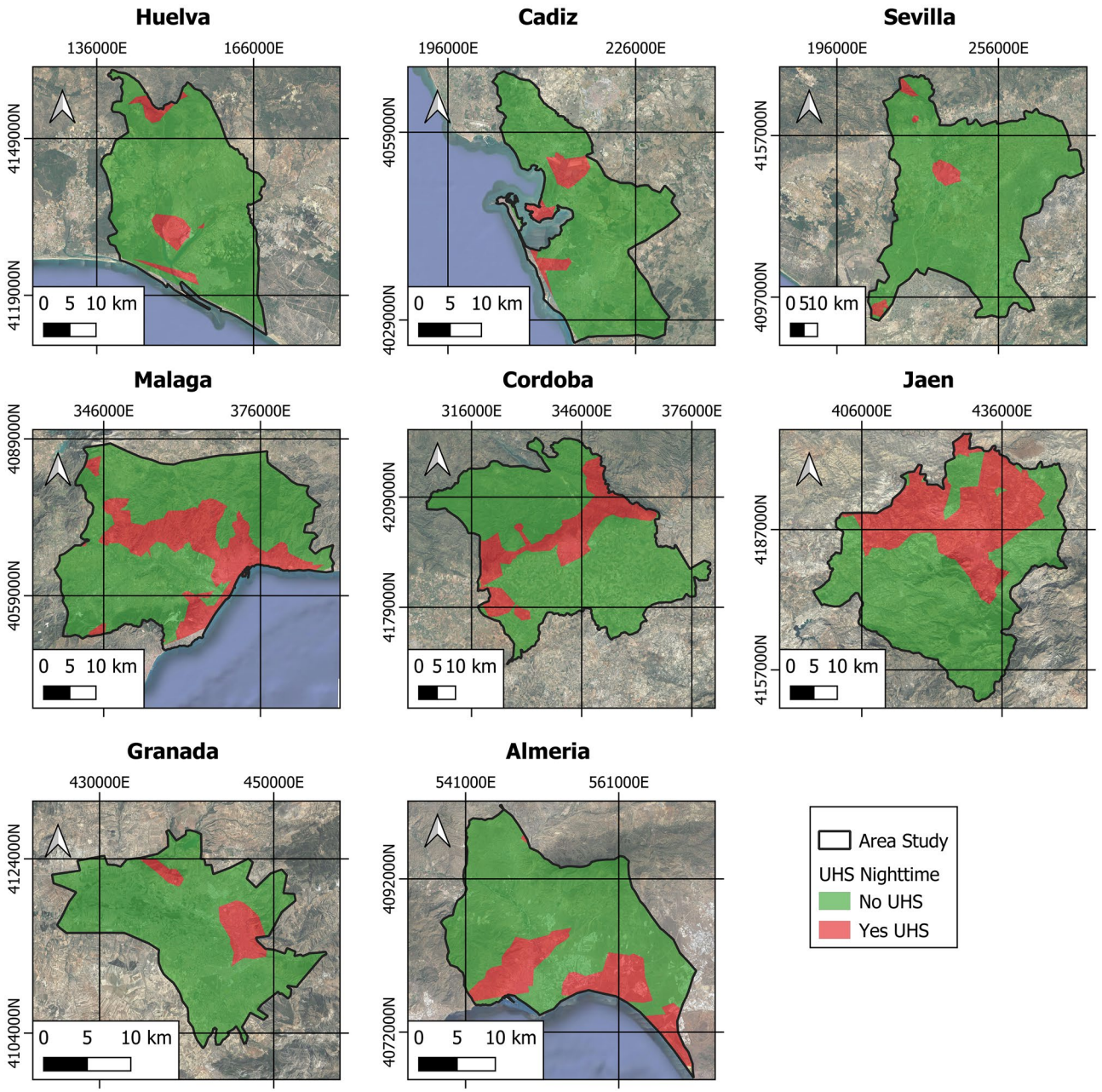

Fig. 9 Variability of the nocturnal UHS of the studied areas

Table 6 LST for the determination of UHS together with the occupation of these zones

	UHS Daytime				UHS Nighttime			
	Non UHS (K)	UHS (K)	UHS (ha)	UHS (%)	Non UHS (K)	UHS (K)	UHS (ha)	UHS (%)
Huelva	< 303.0	≥ 303.0	31906	32.9	< 290.0	≥ 290.0	6542	6.8
Cadiz	< 303.0	≥ 303.0	15949	26.3	< 291.0	≥ 291.0	4734	7.8
Sevilla	< 304.0	≥ 304.0	126747	31.9	< 291.0	≥ 291.0	12500	3.1
Malaga	< 305.0	≥ 305.0	28893	21.7	< 290.0	≥ 290.0	32736	24.6
Cordoba	< 303.1	≥ 303.1	21614	8.1	< 290.3	≥ 290.3	43987	16.5
Jaen	< 302.0	≥ 302.0	26767	15.9	< 288.5	≥ 288.5	43978	26.1
Granada	< 302.1	≥ 302.1	4707	13.1	< 287.0	≥ 287.0	3208	9.0
Almeria	< 305.0	≥ 305.0	8318	22.0	< 290.0	≥ 290.0	11729	7.8

Table 7 UHS occupancy and its relationship with day LULCs

LULC	Huelva	Cadiz	Sevilla	Malaga	Cordoba	Jaen	Granada	Almeria
Rainfed cropland	10.5	44.1	30.8	3.4	35.7			25.0
Mosaic cropland		44.1	46.2	25.9	35.7	34.9	29.7	
Mosaic forest	13.2	11.8	7.7					12.5
Grassland	46.1					18.6		
Shrubland	19.7		15.4	51.7				
Sparce vegetation	10.5			13.8	28.6	46.5	57.4	51.7
Artificial surface				5.2			12.5	10.8

correlations were found for both day- and nighttime between the LST and SUHI variables, as well as between these and the UHS. Yet low correlations were found between UHS and LULC, because the diurnal and nocturnal variability of the UHS does not occur for all the LULC coverages. Thus, in the morning, the UHS are distributed mainly over covers lacking vegetation, or crops, scrub and rainfed areas; at night they correspond to artificial surface covers and without vegetation. Numerous studies using satellite images (Guha et al. 2018; Shahfahad et al. 2021; Sharma et al. 2021) show similar distributions of UHS on the LULCs reviewed, validating the results we obtained. However, other studies locate the UHS by means of an image at the moment of passage of the satellite over the investigated area, not reporting the spatial variability that is evidenced in this work.

Given that the region studied here lies by the Mediterranean Sea basin, the large surface of areas without vegetation extracted from the LULC plans stands out, significantly influencing the development of UHS areas. This could be due to an abandonment of farmland and a progressive decrease in rainfall as a result of climate change (Li et al. 2002; Nicholson and Farrar 1994). The first aspect is documented since the nineteenth century in the Mediterranean basin (Benayas et al. 2007). The agricultural crisis that Spain suffered at the beginning of the twentieth century, the country´s economic development, high production costs, droughts, progressive industrialization and processes of speculation involving these soil types —to transform them into urban terrain and obtain a high profit— are all factors contributing to the increase in this type of coverage (Romero and Martínez 2014). Meanwhile, there has been a decrease in rainfall; according to data from the State Meteorological Agency (AEMET), 17 of the last 32 years have been classified as very dry in Spain. It is therefore evident that climatic conditions alter local land covers, and these in turn alter the patterns of LST and SUHI.

Finally, an important spatial variability and deterioration of the general thermal comfort (UTFVI) is identified between the day and night data of the areas under study. During the mornings, the predominant classes in each territory studied are 3 and 2, while at night the predominant classes are 3 and 4. The distribution of classes in the morning is 1, 2 and 3 in urban areas and 4, 5 and 6 in rural areas, whereas at night classes 1, 2 and 3 are distributed in rural areas and classes 4, 5 and 6 in urban areas. Again evident is the effect of spatial variability reflected in the LST values outlined above. In the morning the LST is higher in rural areas; at night the LST is higher in urban areas owing to waterproof construction materials and high thermal absorption. A number of studies (Guha 2017; Luo and Wu 2021; Majumder et al. 2021; Shahfahad et al. 2021) corroborate significant increases in classes 4, 5 and 6 of the UTFVI index motivated by a growth of urban areas that leads to an increase in the LST. Our results come to support such findings.

Table 8 UHS occupancy and its relationship with night LULCs

LULC	Huelva	Cadiz	Sevilla	Malaga	Cordoba	Jaen	Granada	Almeria
Rainfed cropland	9.2					5.6		
Mosaic cropland							3.0	
Mosaic forest			5.9		1.5	23.5	3.0	3.3
Grassland					5.3			
Shrubland	23.1	25.0	20.0	43.1	18.4		6.1	
Sparce vegetation		15.0		5.2	13.2	16.5	18.5	13.3
Artificial surface	67.7	60.0	74.1	51.7	61.6	54.4	59.4	82.3

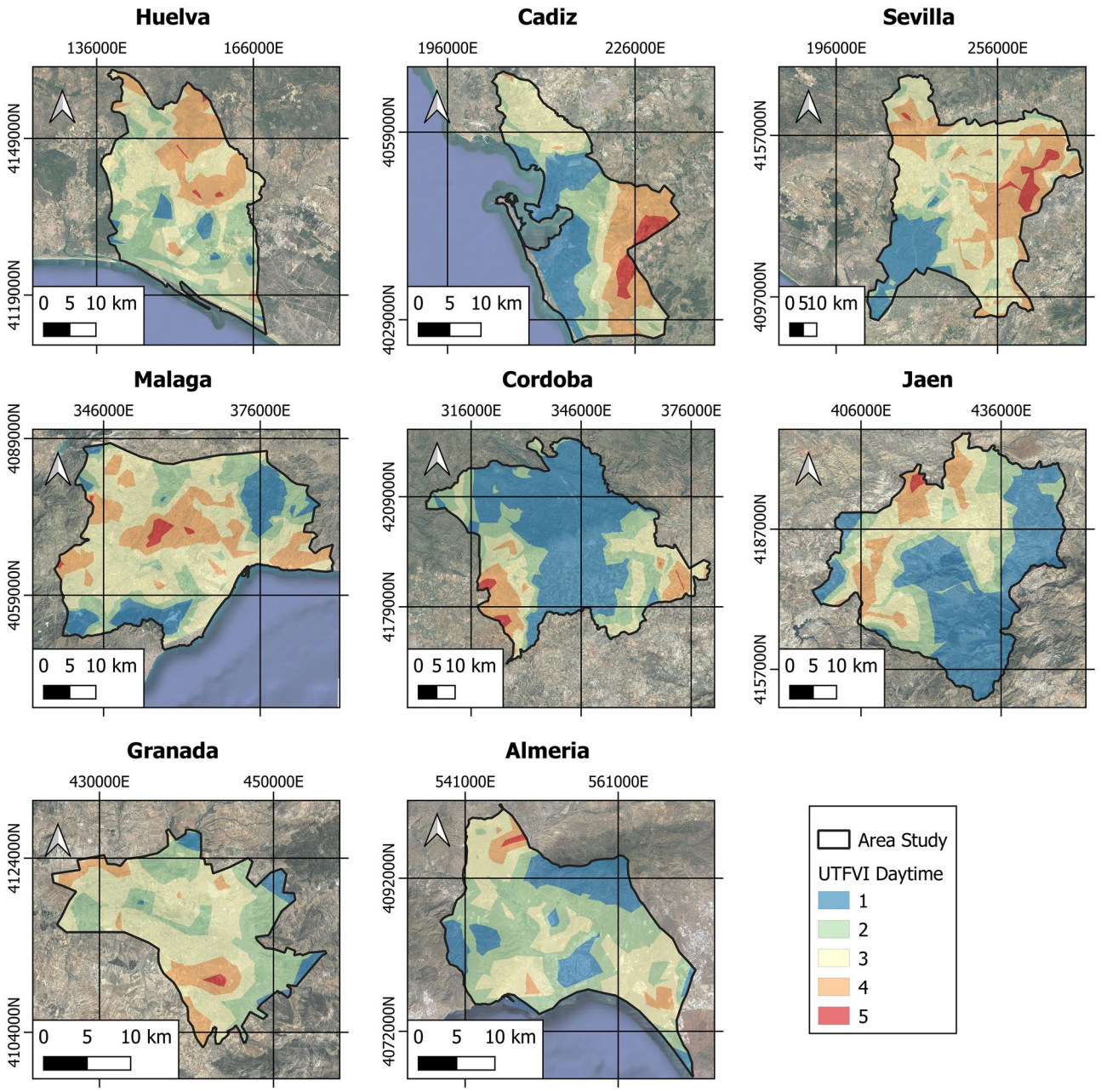

Fig. 10 Variability of the diurnal UTFVI of the studied areas

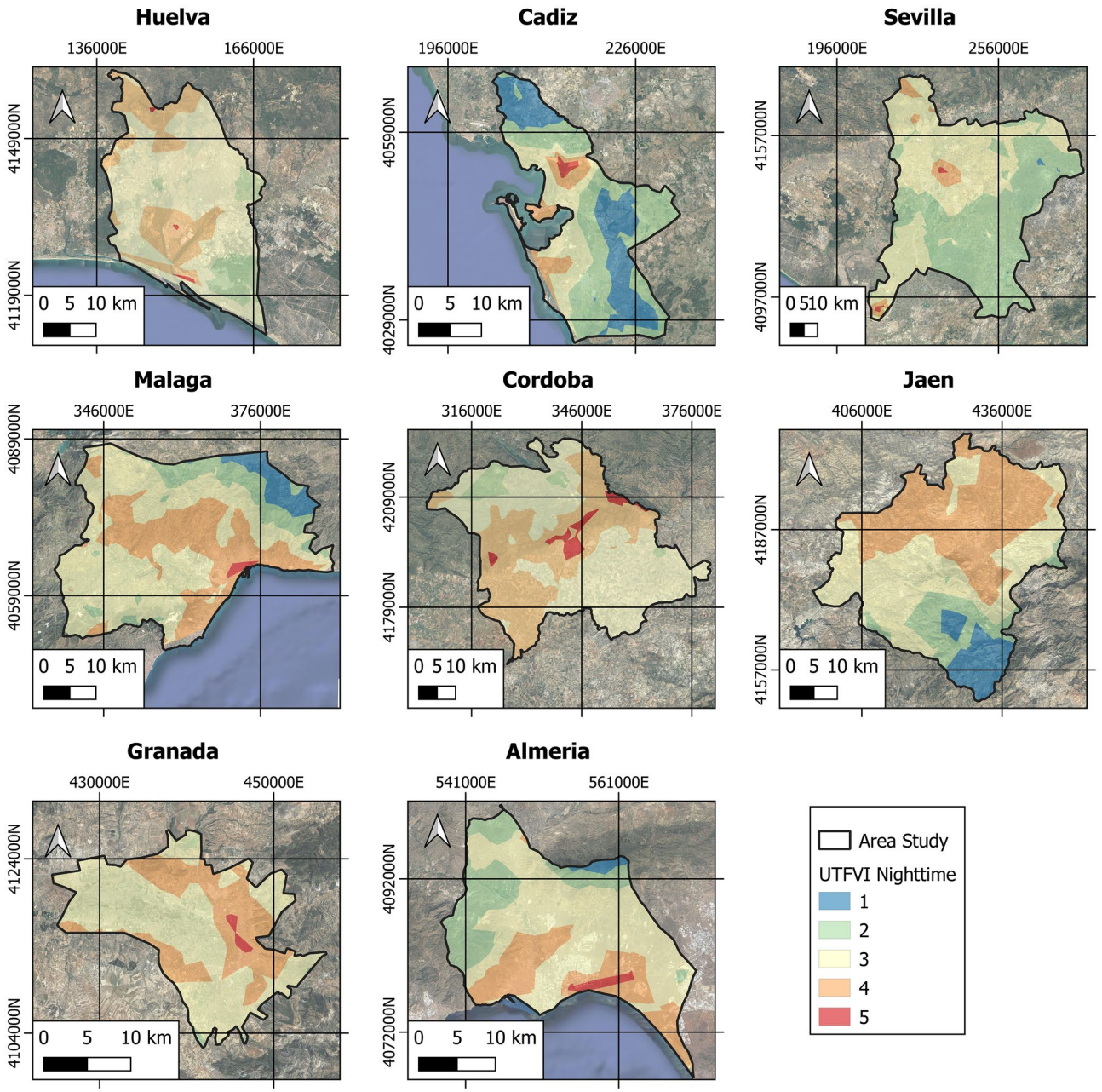

Fig. 11 Variability of the nocturnal UTFVI of the studied areas

Table 9 Daytime UTFVI occupancy

Class	UTFVI	SUHI presence	Ecological index	Huelva	Cadiz	Sevilla	Malaga	Cordoba	Jaen	Granada	Almería
1	< 0	None	Excellent	3.6	28.2	13.1	13.3	53.6	44.8	22.9	21.4
2	0–0.005	Weak	Good	29.8	17.3	8.3	18.9	20.1	19.4	23.5	41.1
3	0.005–0.010	Middle	Normal	44.1	27.2	47.1	46.3	16.6	25.2	35.9	32.8
4	0.010–0.015	Strong	Bad	22.1	22.1	28.6	20.1	8.8	10.0	16.1	4.3
5	0.015–0.020	Stronger	Worse	0.4	5.1	2.9	1.4	1.0	0.5	1.5	0.4
6	> 0.020	Strongest	Worst	0.0	0.0	0.0	0.0	0.0	0.0	0.0	0.0

Table 10 Nighttime UTFVI occupancy

Class	UTFVI	SUHI presence	Ecological index	Huelva	Cadiz	Sevilla	Malaga	Cordoba	Jaen	Granada	Almería
1	< 0	None	Excellent	0.0	27.9	0.2	6.0	0.0	9.4	0.0	21.4
2	0–0.005	Weak	Good	10.7	42.3	49.8	11.5	4.5	11.0	0.7	41.1
3	0.005–0.010	Middle	Normal	62.1	20.2	46.0	52.8	52.9	39.7	65.6	32.8
4	0.010–0.015	Strong	Bad	26.8	8.6	3.7	29.2	39.4	39.9	33.7	4.3
5	0.015–0.020	Stronger	Worse	0.4	1.0	0.2	0.6	3.2	0.0	0.0	0.4
6	> 0.020	Strongest	Worst	0.0	0.0	0.0	0.0	0.0	0.0	0.0	0.0

Table 11 Pearson correlation coefficient LST and LULC

	LULC	$LST_{Daytime}$	$LST_{Nighttime}$
LULC	1.000		
$LST_{Daytime}$	–0.687	1.000	
$LST_{Nighttime}$	0.710	0.173	1.000

Table 12 LULC and LST results

	β	ρ	Sd
$LST_{daytime}$	–0.3963	*0.012**	0.2308
$LST_{nighttime}$	1.018	*0.004***	0.5750
	$R^2 = 0.33$	F = 10.33	Prob > $chi^2 = 0.006$

β Coefficient, *sd* Standard deviation, R^2 Linear regression coefficient, *F* F statistic

Robust standard errors: *p < 0.05, **p < 0.01 and ***p < 0.001

Table 13 Pearson correlation coefficient for LST and SUHI

	$LST_{daytime}$	$LST_{nighttime}$	$SUHI_{daytime}$	$SUHI_{nighttime}$
$LST_{daytime}$	1.000			
$LST_{nighttime}$	0.173	1.000		
$SUHI_{daytime}$	0.715	0.125	1.000	
$SUHI_{nighttime}$	-0.015	0.642	0.123	1.000

Table 14 LST and SUHI daytime results

	β	ρ	sd
$SUHI_{daytime}$	0.7624	*0.000****	0.0345
	$R^2 = 0.37$	F = 476	Prob > $chi^2 = 0.000$

β Coefficient, *sd* Standard deviation, R^2 Linear regression coefficient, *F* F statistic

Robust standard errors: *p < 0.05, **p < 0.01 and ***p < 0.001

Table 15 LST and SUHI nighttime results

	β	ρ	sd
$SUHI_{nighttime}$	0.6631	*0.000****	0.0367
	$R^2 = 0.39$	F = 325	Prob > $chi^2 = 0.000$

β Coefficient, *sd* Standard deviation, R^2 Linear regression coefficient, *F* F statistic

Robust standard errors: *p < 0.05, **p < 0.01 and ***p < 0.001

Table 16 Pearson's correlation coefficient for UHS, LST, SUHI and LULC indices

	UHS daytime	LST daytime	SUHI daytime	UHS nighttime	LST nighttime	SUHI nighttime	LULC
$UHS_{daytime}$	1.000						
$LST_{daytime}$	0.659	1.000					
$SUHI_{daytime}$	0.872	0.715	1.000				
$UHS_{nighttime}$	0.003	–0.049	–0.081	1.000			
$LST_{nighttime}$	0.073	0.273	0.125	0.703	1.000		
$SUHI_{nighttime}$	–0.055	–0.015	0.123	0.823	0.642	1.000	
LULC	–0.011	–0.678	0.238	0.176	0.710	0.249	1.000

Table 17 Results for daytime UHS with daytime LST, daytime SUHI, and LULC

	β	ρ	sd
$LST_{daytime}$	0.0386	*0.035**	0.1832
$SUHI_{daytime}$	0.0903	*0.000****	0.1393
LULC	–0.020	*0.449*	0.0026
	$R^2 = 0.53$	F = 61.85	Prob > $chi^2 = 0.000$

β Coefficient, *sd* Standard deviation, R^2 Linear regression coefficient, *F* F statistic

Robust standard errors: *p<0.05, **p<0.01 and ***p<0.001

Table 18 Results for nighttime UHS with nocturnal LST, nocturnal SUHI and LULC

	β	ρ	sd
$LST_{nighttime}$	0.0367	*0.029**	0.0223
$SUHI_{nighttime}$	0.1768	*0.000***	0.0251
LULC	0.022	*0.196*	0.0017
	$R^2 = 0.48$	F = 289.97	Prob > $chi^2 = 0.000$

β Coefficient, *sd* Standard deviation, R^2 Linear regression coefficient, *F* F statistic

Robust standard errors: *p < 0.05, **p < 0.01 and ***p < 0.001

Conclusions

The area and time period studied (Andalusia, southern Spain, 2021) yield daytime mean LSTs that are greater than nighttime mean LSTs. The daytime LST was higher in rural areas than in urban ones. In contrast, the nocturnal LST was higher in urban areas. This means a high spatial variability is present between day and night readings in the determination of the UHS and the UTFVI index. The diurnal UHS are distributed mainly over LULC covers without vegetation, crops, scrub and rainfed areas, while at night they correspond to artificial surface covers and those without vegetation. It is evident that the transformation of natural and agricultural land into urbanized areas —without vegetation— for speculative purposes would be a main reason behind the high LST and SUHI values, eventually leading to larger areas identified as UHS and a deterioration of thermal comfort. The results of the study come to confirm previous findings.

These results underline the need for significant efforts by the governing public administrations to modify the upward trend of LST, SUHI, UHS and UTFVI values in both urban and rural areas, by formulating new general plans for urban agglomeration. Strategies must promote an increase in green spaces within urban areas, together with the rehabilitation of buildings in historic downtown areas, rather than the development of rural areas in disuse. At the same time, a proliferation of plantations and vegetated areas could reinforce the positive effects of rural areas. This would mean a greater proportion of vegetation cover that receives solar radiation but does not revert it to the atmosphere —as is now the case with impermeable materials and surfaces— to minimize UHS zones and improve the thermal environment.

Authors' contributions The research and writing of the document has been carried out equally by both authors.

Funding Funding for open access publishing: Universidad de Granada/CBUA.

Availability of data and material Not applicable.

Code availability Not applicable.

Declarations

Ethics approval The authors indicates that all the ethical principles governing the publication of a research article in a journal have been followed.

Consent to participate The authors agree to participate in the review process and subsequent publication in the event of such an event.

Consent for publication If the article is accepted, the authors consent to the publication and transfer of the information to the journal.

Conflicts of interest/competing interests The authors indicate that there are no conflicts of interest.

References

Agam N, Kustas WP, Anderson MC, Li F, Colaizzi PD (2007a) Utility of thermal sharpening over Texas high plains irrigated agricultural fields. J Geophys Res Atmos 112(19):1–10. https://doi.org/10.1029/2007JD008407

Agam N, Kustas WP, Anderson MC, Li F, Neale CMU (2007b) A vegetation index based technique for spatial sharpening of thermal imagery. Remote Sens Environ 107(4):545–558. https://doi.org/10.1016/j.rse.2006.10.006

Ahmed S (2018) Assessment of urban heat islands and impact of climate change on socioeconomic over Suez Governorate using remote sensing and GIS techniques. Egypt J Remote Sens Space Sci 21(1):15–25. https://doi.org/10.1016/j.ejrs.2017.08.001

Alcock I, White MP, Lovell R, Higgins SL, Osborne NJ, Husk K, Wheeler BW (2015) What accounts for "England's green and pleasant land"? A panel data analysis of mental health and land cover types in rural England. Landsc Urban Plan 142:38–46. https://doi.org/10.1016/j.landurbplan.2015.05.008

Amindin A, Pouyan S, Pourghasemi HR, Yousefi S, Tiefenbacher JP (2021) Spatial and temporal analysis of urban heat island using Landsat satellite images. Environ Sci Pollut Res 28(30):41439–41450. https://doi.org/10.1007/s11356-021-13693-0

Anjos M, Targino AC, Krecl P, Oukawa GY, Braga RF (2020) Analysis of the urban heat island under different synoptic patterns using local climate zones. Build Environ. https://doi.org/10.1016/j.buildenv.2020.107268

Benayas JMR, Martins A, Nicolau JM, Schulz JJ (2007) Abandonment of agricultural land: An overview of drivers and consequences.

CAB Rev Perspect Agric Vet Sci Nutr Nat Resour 2(057). https://doi.org/10.1079/PAVSNNR20072057
Campbell J (1996) Introduction to Remote Sensing, 2nd edn. The Guilford Press, New York
Chen Y, Li X, Zheng Y, Guan Y, Liu X (2011) Estimating the relationship between urban forms and energy consumption: A case study in the Pearl River Delta, 2005–2008. Landsc Urban Plan 102(1):33–42. https://doi.org/10.1016/j.landurbplan.2011.03.007
Das M, Das A (2020) Assessing the relationship between local climatic zones (LCZs) and land surface temperature (LST) – A case study of Sriniketan-Santiniketan Planning Area (SSPA), West Bengal. India Urban Climate 32:100591. https://doi.org/10.1016/j.uclim.2020.100591
de Castro M, Gallardo C, Jylha K, Tuomenvirta H (2007) The use of a climate-type classification for assessing climate change effects in Europe from an ensemble of nine regional climate models. Clim Change 81(S1):329–341. https://doi.org/10.1007/s10584-006-9224-1
Du J, Xiang X, Zhao B, Zhou H (2020) Impact of urban expansion on land surface temperature in Fuzhou, China using Landsat imagery. Sustain Cities Soc 61(June):102346. https://doi.org/10.1016/j.scs.2020.102346
Dwivedi A, Mohan BK (2018) Impact of green roof on micro climate to reduce Urban Heat Island. Remote Sens Appl Soc Environ 10:56–69. https://doi.org/10.1016/j.rsase.2018.01.003
Emmanuel R, Krüger E (2012) Urban heat island and its impact on climate change resilience in a shrinking city: The case of Glasgow, UK. Build Environ 53:137–149. https://doi.org/10.1016/j.buildenv.2012.01.020
Fang L, Tian C (2020) Construction land quotas as a tool for managing urban expansion. Landsc Urban Plan 195:103727. https://doi.org/10.1016/j.landurbplan.2019.103727
Guha S (2017) Dynamic analysis and ecological evaluation of urban heat islands in Raipur city, India. J Appl Remote Sens 11(03):1. https://doi.org/10.1117/1.jrs.11.036020
Guha S, Govil H, Dey A, Gill N (2018) Analytical study of land surface temperature with NDVI and NDBI using Landsat 8 OLI and TIRS data in Florence and Naples city, Italy. Eur J Remote Sens 51(1):667–678. https://doi.org/10.1080/22797254.2018.1474494
Hidalgo D, Arco J (2021) Modeling of the Urban Heat Island on local climatic zones of a city using Sentinel 3 images: Urban determining factors. Urban Clim 37(September 2020). https://doi.org/10.1016/j.uclim.2021.100840
Hua L, Zhang X, Nie Q, Sun F, Tang L (2020) The impacts of the expansion of urban impervious surfaces on urban heat islands in a coastal city in China. Sustainability 12(2). https://doi.org/10.3390/su12020475
Huryna H, Cohen Y, Karnieli A, Panov N, Kustas WP, Agam N (2019) Evaluation of TsHARP utility for thermal sharpening of Sentinel-3 satellite images using Sentinel-2 visual imagery. Remote Sens 11(19). https://doi.org/10.3390/rs11192304
Karakuş CB (2019) The impact of land use/land cover (LULC) changes on land surface temperature in Sivas City center and its surroundings and assessment of urban Heat Island. Asia-Pac J Atmos Sci 55(4):669–684. https://doi.org/10.1007/s13143-019-00109-w
Kovats RS, Campbell D, Matthies F (2005) Climate change and human health: Estimating avoidable deaths and disease. Risk Anal 25(6):1409–1418. https://doi.org/10.1111/j.1539-6924.2005.00688.x
Labra R (2014) Zero panel data guide. Download: https://U:/Maguilera/Documentos Personales MAGUILERA/Master M3F/Trabajo Fin M3F/Revisión para paper/Referencias/Stata/16_Guia CERO para datos de panel_Un enfoque practico.pdf. Accessed December 2022
Lemus M, Martin J, Moreno MC, Lopez JA (2020) Estimating Barcelona's metropolitan daytime hot and cold poles using Landsat-8 Land Surface Temperature. Sci Total Environ 699:134307. https://doi.org/10.1016/j.scitotenv.2019.134307
Li B, Tao S, Dawson RW (2002) Relations between AVHRR NDVI and ecoclimatic parameters in China. Int J Remote Sens 23(5):989–999. https://doi.org/10.1080/014311602753474192
Li J, Song C, Cao L, Zhu F, Meng X, Wu J (2011) Impacts of landscape structure on surface urban heat islands: A case study of Shanghai, China. Remote Sens Environ 115(12):3249–3263. https://doi.org/10.1016/j.rse.2011.07.008
Li T, Meng Q (2018) A mixture emissivity analysis method for urban land surface temperature retrieval from Landsat 8 data. Landsc Urban Plan 179:63–71. https://doi.org/10.1016/j.landurbplan.2018.07.010
Lin W, Yu T, Chang X, Wu W, Zhang Y (2015) Calculating cooling extents of green parks using remote sensing: Method and test. Landsc Urban Plan 134:66–75. https://doi.org/10.1016/j.landurbplan.2014.10.012
Liu L, Zhang Y (2011) Urban heat island analysis using the landsat TM data and ASTER Data: A case study in Hong Kong. Remote Sens 3(7):1535–1552. https://doi.org/10.3390/rs3071535
Luo H, Wu J (2021) Effects of urban growth on the land surface temperature: a case study in Taiyuan, China. Environ Dev Sustain 23(7):10787–10813. https://doi.org/10.1007/s10668-020-01087-0
Macintyre HL, Heaviside C, Taylor J, Picetti R, Symonds P, Cai XM, Vardoulakis S (2018) Assessing urban population vulnerability and environmental risks across an urban area during heatwaves – Implications for health protection. Sci Total Environ 610–611. https://doi.org/10.1016/j.scitotenv.2017.08.062
Majumder A, Setia R, Kingra PK, Sembhi H, Singh SP, Pateriya B (2021) Estimation of land surface temperature using different retrieval methods for studying the spatiotemporal variations of surface urban heat and cold islands in Indian Punjab. Environ Dev Sustain 23(11):15921–15942. https://doi.org/10.1007/s10668-021-01321-3
McMillin LM (1975) Estimation of sea surface temperatures from two infrared window measurements with different absorption. J Geophys Res 80(36):5113–5117. https://doi.org/10.1029/jc080i036p05113
Mukherjee F, Singh D (2020) Assessing land use-land cover change and its impact on land surface temperature using LANDSAT data: A comparison of two urban areas in India. Earth Syst Environ 4(2):385–407. https://doi.org/10.1007/s41748-020-00155-9
Nicholson SE, Farrar TJ (1994) The influence of soil type on the relationships between NDVI, rainfall, and soil moisture in semiarid Botswana. I. NDVI response to rainfall. Remote Sens Environ 50(2):107–120. https://doi.org/10.1016/0034-4257(94)90038-8
Oke TR (1987) Boundary layer climates. Routledge
Pérez L, Niclòs R, Puchades J, Coll C, Göttsche FM, Valiente JA, Valor E, Galve JM (2021) Validation of sentinel-3 slstr land surface temperature retrieved by the operational product and comparison with explicitly emissivity-dependent algorithms. Remote Sens 13(11). https://doi.org/10.3390/rs13112228
Qiu GY, Zou Z, Li X, Li H, Guo Q, Yan C, Tan S (2017) Experimental studies on the effects of green space and evapotranspiration on urban heat island in a subtropical megacity in China. Habitat Int 68:30–42. https://doi.org/10.1016/j.habitatint.2017.07.009
Remedios J, Emsley S (2012) Sentinel-3 optical products and algorithm definition land surface temperature, 24
Romero A, Martínez C (2014) Usos del suelo y abandono de tierras de cultivo en el Altiplano Jumilla-Yecla (Región de Murcia). Geoecología, Cambio Ambiental y Paisaje: Homenaje Al Profesor José María García Ruiz 479. Download: https://pirineos.revistas.csic.es/index.php/pirineos/article/view/279. Accessed 20 Dec 2022
Rozos E, Makropoulos C, Maksimović Č (2013) Rethinking urban areas: An example of an integrated blue-green approach. Water Sci Technol Water Supply 13(6):1534–1542. https://doi.org/10.2166/ws.2013.140

Ruescas AB, Danne O, Fomferra N, Brockmann C (2016) The land surface temperature synergistic processor in beam: A prototype towards sentinel-3. Data 1(3):1–14. https://doi.org/10.3390/data1030018

Saaroni H, Amorim JH, Hiemstra JA, Pearlmutter D (2018) Urban Green Infrastructure as a tool for urban heat mitigation: Survey of research methodologies and findings across different climatic regions. Urban Clim 24:94–110. https://doi.org/10.1016/j.uclim.2018.02.001

Santamouris M (2020) Recent progress on urban overheating and heat island research. Integrated assessment of the energy, environmental, vulnerability and health impact. Synergies with the global climate change. Energy Build. https://doi.org/10.1016/j.enbuild.2019.109482

Schneider A, Friedl MA, Potere D (2010) Mapping global urban areas using MODIS 500-m data: New methods and datasets based on "urban ecoregions." Remote Sens Environ 114(8):1733–1746. https://doi.org/10.1016/j.rse.2010.03.003

Scolozzi R, Geneletti D (2012) A multi-scale qualitative approach to assess the impact of urbanization on natural habitats and their connectivity. Environ Impact Assess Rev 36:9–22. https://doi.org/10.1016/j.eiar.2012.03.001

Seto KC, Kaufmann RK (2003) Modeling the drivers of urban land use change in the Pearl River Delta, China: Integrating remote sensing with socioeconomic data. Land Econ 79(1):106–121. https://doi.org/10.2307/3147108

Shahfahad S, Rihan M, Hang HT, Bhaskaran S, Rahman A (2021) Modelling urban heat island (UHI) and thermal field variation and their relationship with land use indices over Delhi and Mumbai metro cities. Environ Dev Sustain 0123456789. https://doi.org/10.1007/s10668-021-01587-7

Sharma R, Pradhan L, Kumari M, Bhattacharya P (2021) Assessing urban heat islands and thermal comfort in Noida City using geospatial technology. Urban Clim 35:100751. https://doi.org/10.1016/j.uclim.2020.100751

Sobrino JA, Irakulis I (2020) A methodology for comparing the surface urban heat Island in selected urban agglomerations around the world from Sentinel-3 SLSTR data. Remote Sens 12(12):1–31. https://doi.org/10.3390/RS12122052

Song J, Chen W, Zhang J, Huang K, Hou B, Prishchepov AV (2020) Effects of building density on land surface temperature in China: Spatial patterns and determinants. Landsc Urban Plan 198(March):103794. https://doi.org/10.1016/j.landurbplan.2020.103794

Song J, Lin T, Li X, Prishchepov AV (2018) Mapping urban functional zones by integrating very high spatial resolution remote sensing imagery and points of interest: A case study of Xiamen, China. Remote Sens 10(11). https://doi.org/10.3390/rs10111737

Tepanosyan G, Muradyan V, Hovsepyan A, Pinigin G, Medvedev A, Asmaryan S (2021) Studying spatial-temporal changes and relationship of land cover and surface Urban Heat Island derived through remote sensing in Yerevan, Armenia. Build Environ 187:107390. https://doi.org/10.1016/j.buildenv.2020.107390

Tsou J, Zhuang J, Li Y, Zhang Y (2017) Urban heat island assessment using the landsat 8 data: A case study in Shenzhen and Hong Kong. Urban Sci 1(1):10. https://doi.org/10.3390/urbansci1010010

UNO (2018) 68% of the world population projected to live in urban areas by 2050, says UN. Download: https://www.un.org/development/desa/en/news/population/2018-revision-of-world-urbanization-prospects.html. Accessed 20 Dec 2022

Wu C, Li J, Wang C, Song C, Chen Y, Finka M, La Rosa D (2019) Understanding the relationship between urban blue infrastructure and land surface temperature. Sci Total Environ. https://doi.org/10.1016/j.scitotenv.2019.133742

Xu D, Kang X, Qiu D, Zhuang D, Pan J (2009) Quantitative assessment of desertification using Landsat data on a regional scale - a case study in the Ordos Plateau, China. Sensors 9(3):1738–1753. https://doi.org/10.3390/s90301738

Yang C, Yan F, Zhang S (2020) Comparison of land surface and air temperatures for quantifying summer and winter urban heat island in a snow climate city. J Environ Manag 265(March):110563. https://doi.org/10.1016/j.jenvman.2020.110563

Yang J, Zhou J, Göttsche FM, Long Z, Ma J, Luo R (2020b) Investigation and validation of algorithms for estimating land surface temperature from Sentinel-3 SLSTR data. Int J Appl Earth Obs Geoinf 91(April):102136. https://doi.org/10.1016/j.jag.2020.102136

Yoo C, Han D, Im J, Bechtel B (2019) Comparison between convolutional neural networks and random forest for local climate zone classification in mega urban areas using Landsat images. ISPRS J Photogramm Remote Sens 157(February):155–170. https://doi.org/10.1016/j.isprsjprs.2019.09.009